

# Magnetic Structure of Hydrogen Induced Defects on Graphene

J. O. Sofo,<sup>1</sup> Gonzalo Usaj,<sup>2</sup> P. S. Cornaglia,<sup>2</sup> A. M. Suarez,<sup>1</sup> A. D. Hernández-Nieves,<sup>2</sup> and C. A. Balseiro<sup>2</sup>

<sup>1</sup>*Physics Department, Pennsylvania State University, University Park, PA 16802, USA*

<sup>2</sup>*Centro Atómico Bariloche and Instituto Balseiro, CNEA, 8400 Bariloche, and CONICET, Argentina*

(Dated: submitted, December 2011)

Using density functional theory (DFT), Hartree-Fock, exact diagonalization, and numerical renormalization group methods we study the electronic structure of diluted hydrogen atoms chemisorbed on graphene. A comparison between DFT and Hartree-Fock calculations allows us to identify the main characteristics of the magnetic structure of the defect. We use this information to formulate an Anderson-Hubbard model that captures the main physical ingredients of the system, while still allowing a rigorous treatment of the electronic correlations. We find that the large hydrogen-carbon hybridization puts the structure of the defect half-way between the one corresponding to an adatom weakly coupled to pristine graphene and a carbon vacancy. The impurity's magnetic moment leaks into the graphene layer where the electronic correlations on the C atoms play an important role in stabilizing the magnetic solution. Finally, we discuss the implications for the Kondo effect.

PACS numbers: 73.22.Pr, 81.05.ue, 73.20.-r, 73.20.Hb

## I. INTRODUCTION

The unusual electronic and mechanical properties of graphene<sup>1-6</sup> triggered an intense research activity after the first isolation of individual graphene sheets.<sup>1,7,8</sup> The anomalous charge transport properties of pure graphene are a consequence of its particular sub-lattice symmetry that leads to a band structure with a point-like Fermi surface and a linear dispersion close to the Fermi energy.<sup>9</sup> These properties are responsible for the peculiar low energy excitations, that correspond to massless-Dirac fermions, and for the long electron mean-free path.

The possibility of doping graphene with electrons or holes using external gates, which does not lead to a significant loss of mobility, allows the design of graphene-based devices. Another approach, that is also viewed as a promising way to engineer the band structure and modify its electronic properties, is the controlled adsorption of different types of atoms or molecules on graphene.<sup>10-25</sup> In particular, there has been an increasing interest to incorporate magnetic effects in graphene to use graphene-based devices in spintronics.<sup>14,19,26-30</sup> There are already some advances in this direction, like the injection of spin polarized currents from ferromagnetic electrodes.<sup>26,31,32</sup> An alternative route is the generation of magnetic defects using, for example, adatoms, vacancies or edges. Hydrogen (H) impurities and carbon (C) vacancies are among the simplest and most studied point-like magnetic defects.<sup>33-38</sup>

The problem of H atoms chemisorbed on graphene has been studied by several groups.<sup>11,16,17,23,30,39,40</sup> It is known that H impurities are adsorbed on top of a C atom, forming a covalent bond and locally distorting the honeycomb lattice. There is an increasing consensus that H adatoms acquire a magnetic moment, therefore behaving as magnetic impurities. A simple picture used to describe H on graphene is based on the Anderson model where the localized  $1s$  H orbital is hybridized with the graphene extended states. The intra-atomic Coulomb repulsion at the  $1s$ -orbital, together with the graphene pseudo-gap favors the existence of a local moment at the H impurity.<sup>14,19</sup>

The case of C vacancies is quite different. In the ideal case where the lattice remains undistorted after the removal of a C atom,<sup>27</sup> there is a reduction of the coordination number of the three neighboring atoms that generates a resonant state at the pseudo-gap.<sup>41</sup> The existence of this resonance together with the intra-atomic Coulomb repulsion at the C orbitals naturally leads to the formation of a magnetic moment. This simple picture is consistent with the observation of magnetic, Kondo-like correlations in irradiated samples<sup>42</sup> and enlightens the role of the on-site Coulomb interaction in graphene (from hereon denoted as  $U_C$ ). The parameter  $U_C$  has been estimated to be of the order of a few electronvolts.<sup>43</sup>

A realistic description of impurities on graphene should then include the effects of the electronic correlations in both the impurity and the C orbitals by means of an Anderson-Hubbard like model. Such a model can extrapolate between two different limits: (i) for a small value of the hybridization between the impurity and C orbitals, a magnetic moment that is mainly localized at the impurity orbital can be stable; and (ii) for a large hybridization, bonding and anti-bonding states are shifted away of the low energy region. The effect of these shifts is to effectively remove the  $p_z$  orbital of the hybridized carbon atom from the Fermi energy generating a vacancy-like defect with a magnetic moment localized at the C atoms.

As we will discuss below in detail, we find that the case of a H adatom on graphene is half a way between these two limiting cases. We show that the H impurity creates a defect with a complex magnetic structure where a spin  $S = \frac{1}{2}$  is localized in a linear combination of the H and the neighboring C orbitals showing some of the properties of the vacancy-like defect.

The paper is organized as follows: In Section II we revisit the Density Functional Theory (DFT) for diluted H on graphene and use the results as a guide to estimate realistic effective parameters. In Section III we present an Anderson-Hubbard model and its Hartree-Fock solution is compared with DFT results. In Section IV we show that the results can be interpreted in terms of an effective model of a H-C's cluster embedded in an effective medium and use the Numerical Renormalization Group (NRG) to analyze the stability of the

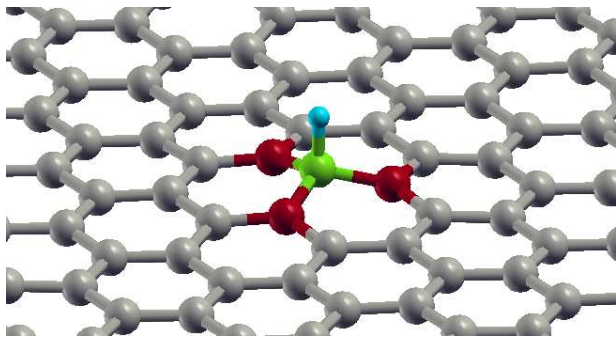


FIG. 1. (Color online) 3D view of a supercell containing 72C atoms (large spheres) and one H impurity (small sphere) on top of a C atom ( $C_0$ ) represented by a green (light gray) sphere. The second nearest-neighbors C atoms ( $C_n$  with  $n = 1, 2, 3$ ) are represented by red (dark gray) spheres.

magnetic solution. Finally, a summary and the conclusions are presented in Section V.

## II. DFT RESULTS

We consider a graphene layer with a low concentration of H atoms. We calculate the spin dependent electronic structure of systems with a unit cell of  $N$  C atoms and one H atom where  $N$  ranges between 32 and 72. Our DFT calculations were done with a plane wave basis as implemented in the VASP code<sup>44</sup> and the cutoff energy was set to 400eV. The core electrons were treated with a frozen core projector augmented wave (PAW) method.<sup>45,46</sup> The frozen core pseudopotential for carbon used a core radius for the  $s$  partial waves of 1.20 a.u. and 1.5 a.u. for the  $p$  channel. All partial waves for H were treated with a cutoff radius of 1.10 a.u.. We use the PBE generalized gradient approximation to treat the exchange and correlations.<sup>47,48</sup> To correct for the dipole moment generated in the cell and to improve convergence with respect to the periodic cell size, monopole and dipole corrections were considered.<sup>49</sup>

Figure 1 shows the relaxed structure of a supercell of 72 C atoms containing one H adatom. After minimizing the total energy with respect to the coordinates of all atoms in the unit cell, we find a H induced distortion consisting of a puckering of the hybridized carbon atom. The distortion is due to the modification of the electronic structure of the C atom bonded with the H adatom that changes from an  $sp^2$  configuration to an  $sp^3$ -like configuration after the hybridization with the H orbital. In the following, we use the label  $C_0$  for the C atom directly bonded to the H impurity.  $C_0$  is represented by a green (light gray) sphere in Fig. 1. The second nearest-neighbors C atoms are represented by red (dark gray) spheres and are labeled as  $C_n$  with  $n = 1, 2, 3$ .

Partial densities of states (PDOS) are calculated using a projector scheme provided in the PAW implementation of VASP4.6 when LORBIT=11. The PDOS corresponding to the H atom shows the existence of a spin-split resonant state close to the Fermi level, see Fig. 2(a). This induces a total magnetic

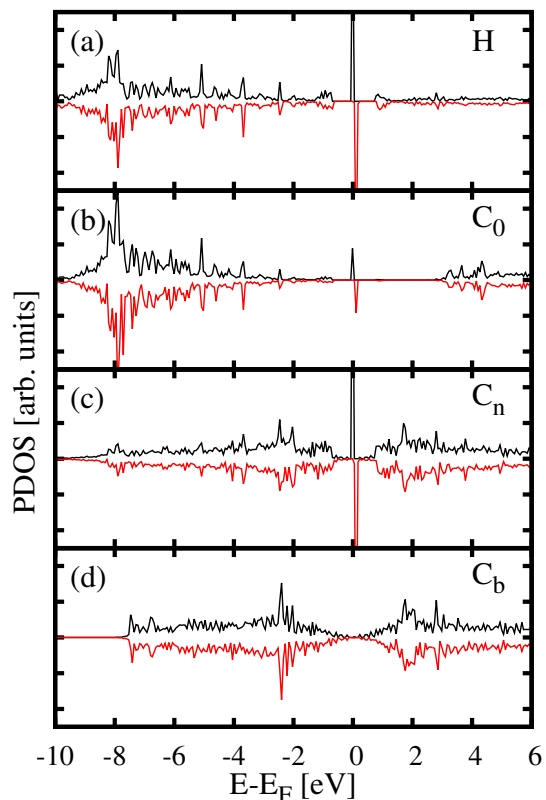


FIG. 2. (Color online) Partial density of states (PDOS) for the undoped case projected on (a) the H atom, and the  $p_z$ -orbitals of (b) the nearest-neighbor carbon atom ( $C_0$ ), (c) one of the second nearest-neighbors carbon atoms ( $C_n$ ), and (d) for a C atom located far from the adatom. For each case case both the majority and minority spin PDOS are plotted. A clear spin-polarized resonant state near the Fermi level  $E_F$  is observed in Figs. 2(a) and 2(c).

moment of  $\approx 0.49 \mu_B/\text{cell}$  localized around the impurity. The covalent bond with the H induces a spin-polarization in the surrounding C atoms. The spin-polarization is small in the nearest C atom ( $C_0$ ), as shown in Fig. 2(b) where there is only a small spin-polarized peak close to the Fermi level. The magnetic moment is larger at the second nearest-neighbor C atoms ( $C_n$ ) as can be appreciated in the strong spin-polarization of the  $p_z$  orbitals of these atoms, see Fig. 2(c). The spin-polarization induced by the H adatom on the graphene layer tends to decrease at large distances from the absorption point, and far from the H adatom the PDOS corresponding to the  $p_z$  orbitals of the C atoms [Fig. 2(d)] shows a Dirac point similar to the behavior of the C atoms in pristine graphene.

The H adatom induces a magnetic moment and charge redistribution on the surrounding carbon atoms that can be analyzed by monitoring the atomic charge and magnetization as a function of the distance between the H atom and the graphene plane ( $R$ ). This is shown in Fig. 3. The vertical dashed line marks the equilibrium position. The charge of the H atom increases, and its magnetic moment decreases, as it approaches the graphene sheet as shown in Figs. 3(a) and 3(b). The opposite occurs for the second nearest-neighbors  $C_n$  atoms (red short-dashed lines) in Figs. 3(c) and 3(d), i.e., the charge of

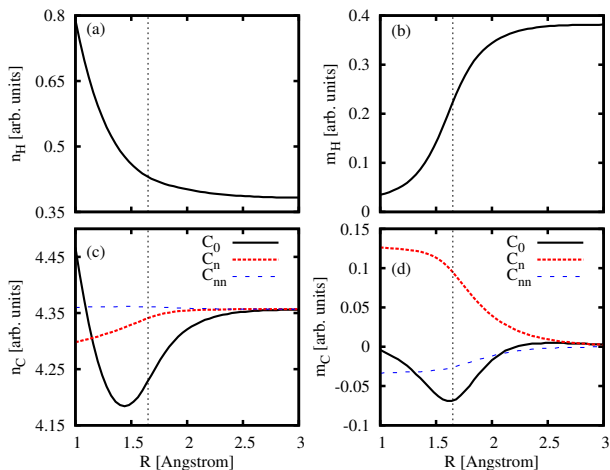


FIG. 3. (Color online) Charge and magnetization of the most relevant atoms as a function of the distance  $R$  between the H atom and the graphene sheet. The equilibrium position of the adatom is indicated by a vertical dashed line. Notice how the charge (magnetization) of the H atom increases (decreases) as it approaches the graphene sheet. The opposite occurs for the  $C_n$  atoms (red short-dashed lines). Both the charge and the magnetization of the  $C_0$  atom have a minimum close to the equilibrium position.

the  $C_n$  atoms decreases while the magnetization increases as the H atom approaches the graphene sheet. A different behavior can be observed at the absorption site, the  $C_0$  atom. In this case, the charge shows a minimum and the absolute value of the magnetization a maximum close to the equilibrium position.

Far from the absorption site, the perturbation induced by the H atom is smaller and alternates its magnitude between sub-lattices—it is larger on the sub-lattice corresponding to the  $C_n$  atoms. For example, the charge of the third nearest-neighbors [ $C_{nn}$  atoms in Fig. 3(c)] is almost independent of the position of the adatom, whereas the magnetization of these atoms only changes slightly compared with the changes in the magnetization of the  $C_n$  atoms [compare the red short-dashed and blue dashed lines in Fig. 3(d)]. This shows that the H atom generates a charge redistribution mostly on the same sub-lattice of the absorption site and predominantly at the neighboring C atoms, those that were highlighted with different colors in Fig. 1. As we will see in the next sections, the behavior of the system can be described by a simple model that takes into account the  $e-e$  correlations only in these atoms and connects them with the rest of the graphene lattice described with a simpler approximation.

As was found recently for the case of fluorine adatoms,<sup>50</sup> the nature of the chemical bonding of adatoms on graphene can change strongly with electron and hole doping. When graphene is electron-doped, the  $C_0$  atom bonded to the F atom retracts back to the graphene plane and for high doping its electronic structure corresponds to nearly a pure  $sp^2$  configuration, see Ref. [50] for details. The situation is different for the electron doping of graphene with H impurities. To simulate electron doping we add one electron per unit cell. The extra charge is compensated with a uniform charge background. The results obtained are shown in Fig. 4. The most

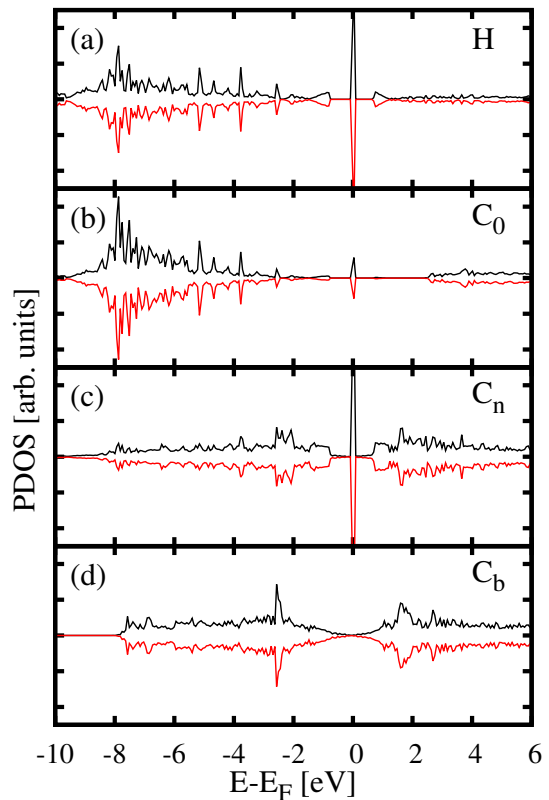


FIG. 4. (color online) Same as Fig. 2 but doped with an extra electron in the unit cell. Notice the absence of spin-polarization in the system after electron doping.

important difference between Figs. 2 and 4 is the absence of spin-polarization in the system after electron doping. As we can see, a similar electronic structure with well defined peaks at the Fermi level is observed but neither the H atom, nor the  $C_0$  or  $C_n$  atoms show spin-polarization—see Figs. 4(a)-4(c). This dependence between gate doping and magnetic moment highlights the delicate interplay between electron correlations and localization in graphene with chemisorbed adatoms. In the following, we use our DFT results as a guide to formulate a theory that goes beyond the mean field level.

### III. ANDERSON-HUBBARD MODEL

In order to interpret the DFT results and give a more physical picture of the magnetic structure of the defect we use a simple Anderson-Hubbard (AH) model given by

$$\hat{H} = \hat{H}_{\text{graph}} + \hat{H}_{\text{imp}} + \hat{H}_{\text{hyb}}, \quad (1)$$

where  $\hat{H}_{\text{graph}}$  describes the  $\pi$ -bands of the graphene sheet,

$$\hat{H}_{\text{graph}} = - \sum_{\langle i,j \rangle \sigma} t_{ij} c_{i\sigma}^\dagger c_{j\sigma} + U_C \sum_i \left( \hat{n}_{i\uparrow} - \frac{1}{2} \right) \left( \hat{n}_{i\downarrow} - \frac{1}{2} \right), \quad (2)$$

here  $c_{i\sigma}^\dagger$  creates an electron with spin  $\sigma$  at site  $i$  of the graphene lattice, the first sum runs over nearest neighbors,

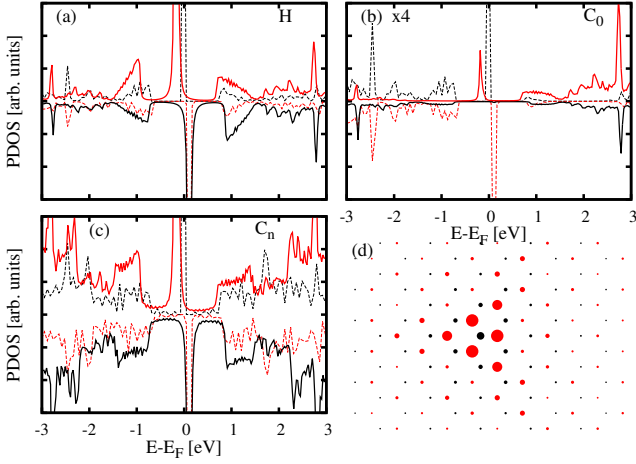


FIG. 5. (color online) Comparison between the DFT PDOS (dashed line) projected onto the  $p_z$  orbitals and the Hartree-Fock (solid line) results obtained with the full AH model. In both cases we use a 72C atoms unit cell. The right bottom panel shows the spatial distribution of the magnetization on the C atoms obtained with the AH model for a unit cell of 288 C atoms where finite size effects are negligible.

$U_C$  is the Coulomb repulsion in the carbon atoms and  $\hat{n}_{i\sigma} = c_{i\sigma}^\dagger c_{i\sigma}$  is the number operator of site  $i$ . The H impurity, which is bounded to the  $C_0$  atom located at site  $i = 0$ , is described by

$$\hat{\mathcal{H}}_{\text{imp}} = \sum_{\sigma} \varepsilon_H h_{\sigma}^\dagger h_{\sigma} + U_H h_{\uparrow}^\dagger h_{\uparrow} h_{\downarrow}^\dagger h_{\downarrow} \quad (3)$$

where  $h_{\sigma}^\dagger$  creates an electron with spin  $\sigma$  at the  $1s$  orbital of the H impurity with energy  $\varepsilon_H$  and intra-atomic Coulomb repulsion  $U_H$ . The impurity-graphene interaction includes a one-body hybridization  $V$  and a distortion-induced shift of the  $C_0$  carbon energy  $\varepsilon_0$ ,

$$\hat{\mathcal{H}}_{\text{hyb}} = \varepsilon_0 \hat{n}_0 - V \sum_{\sigma} (c_{0\sigma}^\dagger h_{\sigma} + h_{\sigma}^\dagger c_{0\sigma})$$

with  $\hat{n}_0 = c_{0\uparrow}^\dagger c_{0\uparrow} + c_{0\downarrow}^\dagger c_{0\downarrow}$ . In what follows we assume that the hopping matrix elements  $t_{ij}$  with  $i, j \neq 0$  are all equal to  $t = 2.8$  eV while  $t_{0j} = t_{j0}$  is reduced by the distortion. The energy of the hybridized carbon orbital is given by  $\varepsilon_0 = A^2(\varepsilon_s - \varepsilon_p)$ , where  $\varepsilon_s \sim -8$  eV and  $\varepsilon_p \equiv 0$  are the energies of the  $s$  and  $p$  carbon orbitals, respectively, while  $A$  is a constant that parametrizes the deformation of the  $sp^2$  bonding of  $C_0$ .<sup>15</sup> This expression interpolates between  $A = 0$  for the  $sp^2$  and  $A = \frac{1}{2}$  for the  $sp^3$  configurations. From the DFT results for the PDOS of a H far from the graphene surface we obtain that  $\varepsilon_H \sim -1.4t$  and  $U_H \sim 2.8t$  while we set  $U_C = t$ . Guided by the DFT results we take  $t_{0j} = t_0 = 0.6t$ ,  $\varepsilon_0 = -0.7t$  and  $V = 2t$ .

Figure 5 shows a comparison of the DFT results for the PDOS projected onto the  $p_z$  orbitals with those obtained with the AH model within the Hartree-Fock (HF) approximation. In both cases we used a cell of 72 C atoms to facilitate the comparison. There is a good qualitative agreement between both methods, which indicates that the chosen effective AH

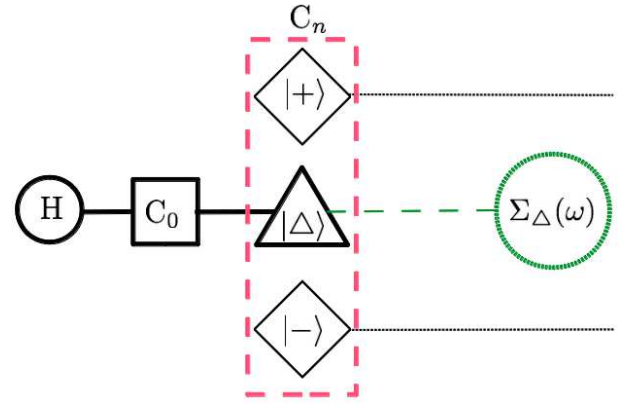


FIG. 6. Schematic representation of the MAHM. The H impurity, the  $C_0$  atom and the state  $|\Delta\rangle$  are treated exactly while the rest of the C atoms are treated as a non-interacting reservoir represented by the self-energy  $\Sigma_{\Delta}(\omega)$ . The capacitive coupling to the  $|\pm\rangle$  states is taken into account only through a mean field approximation (see text).

parameters are adequate for capturing the relevant aspects of the problem—it should be emphasized that we do not intend to fit the parameters but find a reliable range of values for them. The overall qualitative agreement include some features related to the finite size of the cell as, for example, the appearance of gap-like and sharp peak structures. This is a consequence of the interference effects introduced by the periodic array of impurities (all in the same sub-lattice). Within our TB model, such an effect can be eliminated, without much numerical effort, by increasing the size of the unit cell. Fig. 5(d) shows the spatial profile of the magnetization on a cell containing 288 C atoms, which shows a triangular symmetry characteristic of an isolated impurity.

### A. Minimal Anderson-Hubbard model

The AH model presented above can be further reduced to a much simpler model that still captures the relevant aspects of the problem, allows to consider a single isolated impurity, greatly reduces the numerical work, and reproduces to an excellent accuracy the results of the full HF approach obtained with large unit cells. We first note that within the HF approximation, the presence of the H impurity generates a small charge redistribution mainly on its neighboring C atoms. Namely, in the  $C_0$  atom and the three next nearest-neighbors,  $C_n$  with  $n = 1, 2, 3$  (see Fig. 1). Therefore, it is sufficient to limit ourselves to consider a small cluster embedded in an effective medium where the energies of the  $p_z$  orbitals are fixed and the occupation numbers are solved self-consistently in the cluster. This approximation is numerically simpler as the self-consistent equations can be expressed in terms of integrals of analytical functions. Moreover, based on this approximation, the reduced Hamiltonian can be treated using more powerful numerical tools like exact diagonalization or the Numerical Renormalization Group (NRG) presented in the next section.

To illustrate the procedure, let us first consider the one-body part of  $\hat{\mathcal{H}}$ . Due to the hexagonal structure of the lattice, the  $C_0$  atom only couples to the symmetric combination of the  $p_z$  orbitals of its nearest neighbor carbon atoms ( $C_n$ ). We denote that state as  $|\Delta\rangle$  and the corresponding fermionic operator as  $c_{\Delta\sigma}^\dagger = \sum_n c_{n\sigma}^\dagger/\sqrt{3}$  where  $n = 1, 2, 3$  labels the  $C_n$  atoms (we will also refer to this state as  $C_\Delta$ ). The other two orthogonal linear combinations of the  $C_n$   $p_z$ -orbitals, denoted by  $|\pm\rangle$ , are not directly coupled to  $C_0$ . Furthermore, because of the symmetry of the hexagonal lattice, the states  $|\Delta\rangle$  and  $|\pm\rangle$

are not coupled by the rest of the lattice either. As a result, the one-body terms of  $\hat{\mathcal{H}}$  can be separated into three decoupled parts—this is schematically shown in Fig. 6.

Hence, for calculating the properties of the H impurity, the  $C_0$  atom and  $C_\Delta$ , it is sufficient to consider a reduced Hamiltonian for the reduced system (see Fig. 6) and include the rest of the lattice as an effective self-energy  $\Sigma_\Delta(\omega)$ —the calculation is presented in the appendix. More explicitly, the one-body Green function of the reduced system can be written as  $\mathbf{G}(\omega) = [\omega\mathbf{I} - \mathcal{H}_r(\omega)]^{-1}$  with

$$\mathcal{H}_r(\omega) = \begin{pmatrix} \varepsilon_H & V & 0 & 0 & 0 & 0 \\ V & \varepsilon_0 & \sqrt{3}t_0 & 0 & 0 & 0 \\ 0 & \sqrt{3}t_0 & \varepsilon_\Delta + \Sigma_\Delta(\omega) & 0 & 0 & 0 \\ 0 & 0 & 0 & \varepsilon_+ + \Sigma_+(\omega) & 0 & 0 \\ 0 & 0 & 0 & 0 & \varepsilon_- + \Sigma_-(\omega) & 0 \end{pmatrix}, \quad (4)$$

where we have included the possibility that the  $C_n$  atoms have a different energy than the rest of the C atoms of the graphene lattice (and included the  $|\pm\rangle$  states for completeness). So far this is an exact procedure. The addition of the Coulomb interactions  $U_H$  and  $U_C$  *only* in  $C_0$  can still be treated in a similar way, provided we use the appropriate method, as the rest of the system remains a non-interacting fermionic bath and it can still be represented by  $\Sigma_\Delta(\omega)$ . This is no longer true when interactions are included in the rest of the C atoms. We will argue, however, that for a qualitative understanding it is sufficient, and important, to take into account the  $U_C$  interaction *only* on  $C_0$  and the  $C_n$  ( $n = 1, 2, 3$ ) atoms. We will refer to this model as the Minimal Anderson-Hubbard Model (MAHM).

At the level of the HF approximation, the Coulomb repulsion  $U_C \sum_{i=1,2,3} (\hat{n}_{i\uparrow} - \frac{1}{2})(\hat{n}_{i\downarrow} - \frac{1}{2})$  shifts the energy of the states  $|\Delta\rangle$  and  $|\pm\rangle$  preserving the form of the effective Hamiltonian  $\mathcal{H}_r(\omega)$  for each spin projection and then the propagators. The spin dependent self-consistent Green function  $\tilde{\mathbf{G}}_\sigma$  of the system is obtained from Eq. (4) with the self-consistent energies  $\tilde{\varepsilon}_H^\sigma = \varepsilon_H + U_H(\langle \hat{n}_{H\bar{\sigma}} \rangle - \frac{1}{2})$ ,  $\tilde{\varepsilon}_0^\sigma = \varepsilon_0 + U_C(\langle \hat{n}_{0\bar{\sigma}} \rangle - \frac{1}{2})$ , and

$$\tilde{\varepsilon}_\Delta^\sigma = \varepsilon_\Delta + U_C \left( \frac{\langle \hat{n}_{\Delta\bar{\sigma}} \rangle + \langle \hat{n}_{+\bar{\sigma}} \rangle + \langle \hat{n}_{-\bar{\sigma}} \rangle}{3} - \frac{1}{2} \right) \quad (5)$$

with  $\bar{\sigma} = -\sigma$ . We have tested the validity of the MAHM by comparing the PDOS of the H, the  $C_0$ , and the  $C_n$  atoms with those obtained with the full model which includes the  $U_C$  interactions everywhere. The agreement between both approaches is excellent, provided the unit cell used in the later case is large enough for the finite cell size effects to be negligible. It is also worthy to emphasize that the MAHM leads to a magnetic structure similar to the one shown in Fig. 5(d), which indicates that much of the observed antiferromagnetic structure is related to Friedel oscillations.

It is interesting to compare results of the MAHM with those of DFT. For that purpose, we plot in Fig. 7(a) the magnetiza-

tion of the H,  $C_0$  and  $C_n$  atoms as a function of the hybridization  $V$  for two different values of  $\varepsilon_H$ . These results should be compared with those in Fig. 3. We clearly see that the MAHM is able to capture the most relevant features of the DFT results. Namely, that the magnetic state of the impurity is somewhere in between a pure adatom state ( $V \ll t$ ), where the magnetization is mainly localized at the H atom, and a vacancy state ( $V \rightarrow \infty$ ), where a substantial amount of magnetization has been transferred to the  $C_n$  atoms (mainly dominated by the  $|\Delta\rangle$  state). For a quantitative comparison of the results we have to consider the fact that in the DFT approach the lattice is relaxed for each H-graphene distance and consequently other parameters, like  $\varepsilon_0$  and  $t_0$ , also depend on the distance.

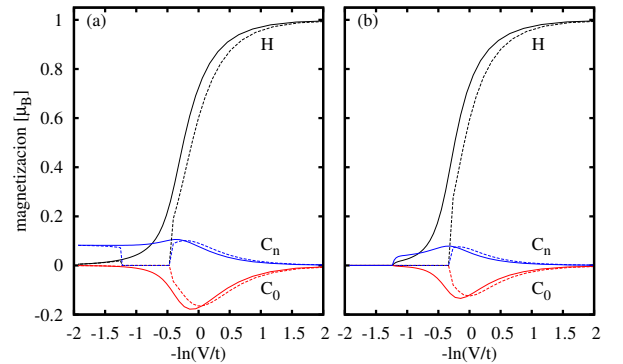


FIG. 7. (color online) Site magnetization as a function of the hybridization  $V$  between the H and  $C_0$  atoms obtained within the MAHM for two different values of  $\varepsilon_H$ :  $\varepsilon_H = 1.29t$  (solid lines) and  $\varepsilon_H = 0.7t$  (dashed lines) and for  $U_C = t$  (a) and  $U_C = 0$  (b). Notice that the simple model is able to capture the general trend of the spatial distribution of the magnetic structure (compare with Fig. 3). The presence of  $U_C$  not only induces some magnetization of the  $C_n$  atoms for large  $V$  but can also lead to a re-entry behavior of the magnetization.

Figure 7(b) shows the same parameters but in the absence of the  $e$ - $e$  interaction on the C atoms. Clearly, the  $U_C$  interaction plays an important role in the case of large  $V$  (vacancy-like state), being responsible of the re-entry behavior observed in Fig. 7(a).

Before discussing the effect of the interactions beyond the HF approximation, we note that for  $\omega \rightarrow 0$  the self-energy  $\Sigma_\Delta(\omega) \sim \alpha\omega \ln|\omega| - i\sqrt{3}|\omega|$ , and the spectral density of the  $|\Delta\rangle$  state presents a divergence at the Dirac point,  $-\text{Im}(g_\Delta) = -\text{Im}(1/[\omega - \Sigma_\Delta(\omega)])$ . This is precisely the vacancy state (projected onto the  $|\Delta\rangle$  state) that has been extensively discussed in the literature.<sup>41,51</sup> This singular DOS is what makes the  $|\Delta\rangle$  state unstable against the formation of a localized magnetic moment when the interactions are included. Conversely, the  $\Sigma_\pm(\omega)$  self-energies diverge at the Dirac point and the spectral densities of the  $|\pm\rangle$  states show a pseudo-gap at low energies (see the appendix). In view of this, one can expect that the main role of the  $U_C$  interaction at low energies will manifest through the weakest coupled state  $|\Delta\rangle$ . Therefore, we only keep the  $U_C/3 (\hat{n}_{\Delta\uparrow} - \frac{1}{2}) (\hat{n}_{\Delta\downarrow} - \frac{1}{2})$  part of

$$\begin{aligned} \hat{\mathcal{H}}_{\text{cluster}} = & \varepsilon_H \hat{n}_H + U_H h_\uparrow^\dagger h_\uparrow h_\downarrow^\dagger h_\downarrow + \varepsilon_0 \hat{n}_0 + U_C \left( \hat{n}_{0\uparrow} - \frac{1}{2} \right) \left( \hat{n}_{0\downarrow} - \frac{1}{2} \right) + \bar{\varepsilon}_\Delta \hat{n}_\Delta + \frac{U_C}{3} \left( \hat{n}_{\Delta\uparrow} - \frac{1}{2} \right) \left( \hat{n}_{\Delta\downarrow} - \frac{1}{2} \right) \\ & - V \sum_\sigma (c_{0\sigma}^\dagger h_\sigma + h_\sigma^\dagger c_{0\sigma}) - \sqrt{3}t_0 \sum_\sigma (c_{\Delta\sigma}^\dagger c_{0\sigma} + c_{0\sigma}^\dagger c_{\Delta\sigma}) \end{aligned} \quad (7)$$

and  $\hat{\mathcal{H}}_{\text{band}}$  and  $\hat{\mathcal{H}}_{\text{hyb}}$  describe a band with a pseudo-gap at the Dirac point and the coupling to the  $|\Delta\rangle$  state

$$\hat{\mathcal{H}}_{\text{band}} = \sum_{\nu\sigma} \varepsilon_\nu f_{\nu\sigma}^\dagger f_{\nu\sigma} \quad (8)$$

$$\hat{\mathcal{H}}_{\text{hyb}} = \sum_{\nu\sigma} t_\nu (f_{\nu\sigma}^\dagger c_{\Delta\sigma} + c_{\Delta\sigma}^\dagger f_{\nu\sigma}), \quad (9)$$

that can be rewritten as

$$\hat{\mathcal{H}}_{\text{hyb}} = \sqrt{2}t \sum_\sigma (f_{0\sigma}^\dagger c_{\Delta\sigma} + c_{\Delta\sigma}^\dagger f_{0\sigma}). \quad (10)$$

where  $f_{0\sigma}^\dagger = \frac{1}{\sqrt{2}t} \sum_\nu t_\nu f_{\nu\sigma}$ , creates an electron on a symmetric combination of H's third-nearest-neighbor C atoms.

It is instructive to start the analysis by looking at the many-body states of the isolated cluster. For undoped graphene ( $\mu = 0$ ), we take  $\bar{\varepsilon}_\Delta = 0$ ,  $U_H \sim 3t$  and  $U_C = t$  as in the previous sections but take  $\varepsilon_0 = 0$  in what follows to simplify the analysis (taking  $\varepsilon_0 \neq 0$  introduces an electron-hole asymmetry which is not relevant at this point).

We diagonalize  $\hat{\mathcal{H}}_{\text{cluster}}$  in the different charge sectors for different values of  $\varepsilon_H$  and  $V$ . Figure 8 shows the regions of stability of the different charge states in the  $[\varepsilon_H, V]$  plane. For  $\varepsilon_H \sim -U_H/2$  the ground state is always a 3-particle state with spin  $S = 1/2$ . The region of stability of the magnetic states as a function of  $\varepsilon_H$  shows a narrowing for  $V \sim 2t$ . For

the interaction between the  $C_n$  ( $n = 1, 2, 3$ ) atoms in what follows and neglect the rest.

Under these assumptions the reduced Hamiltonian (MAHM) describes a correlated three-site cluster, given by the H, the  $C_0$  and the  $|\Delta\rangle$  orbitals, embedded in an effective medium with a pseudo-gap described by  $\Sigma_\Delta(\omega)$  — the mean field charge interaction between the  $|\Delta\rangle$  and the  $|\pm\rangle$  orbitals that tends to keep the charge neutrality of the  $|\Delta\rangle$  state can be included through an effective site energy  $\bar{\varepsilon}_\Delta$ . In the next section we analyze the properties of this model.

#### IV. EXACT DIAGONALIZATION AND NRG RESULTS

The reduced Hamiltonian has the form

$$\hat{\mathcal{H}}_R = \hat{\mathcal{H}}_{\text{cluster}} + \hat{\mathcal{H}}_{\text{band}} + \hat{\mathcal{H}}_{\text{hyb}}, \quad (6)$$

where

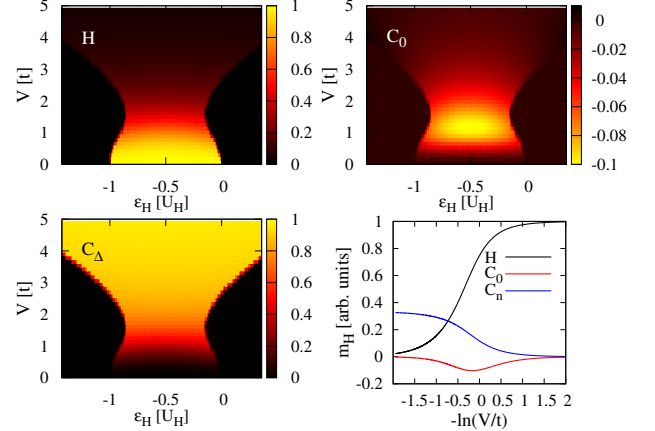


FIG. 8. (Color online) Color maps showing the magnetization of the H,  $C_0$  and  $C_\Delta$  atoms as a function of the orbital energy of the H atom,  $\varepsilon_H$  and the adatom hybridization  $V$  as obtained from the exact diagonalization of  $\hat{\mathcal{H}}_{\text{cluster}}$ . The right lower panel shows the magnetization for  $\varepsilon_H = -U_H/2$  (note that here the magnetization of  $C_n$  is plotted).

$V < 2t$ , the magnetic moment is localized mainly at the H orbital while for  $V > 2t$  it is transferred to the  $|\Delta\rangle$  state. Note that, as the hybridization increases, the spin is transferred directly from the H atom to the  $|\Delta\rangle$  orbitals, in agreement with the DFT and HF results. This is more clearly seen in Fig. 8(d) where the magnetization of the H,  $C_0$  and  $C_n$  atoms is plotted

as a function of  $\ln(V/t)$  for  $\varepsilon_H = -U_H/2$  (this is equivalent to plot it as a function of the H–C<sub>0</sub> distance if an exponential dependence of  $V$  is assumed). In agreement with the previous results, the magnetic moment is transferred to the C orbitals as the hybridization increases.

From these exact results we can now calculate the Kondo coupling constant  $J$ . This is done in the standard way, eliminating high energy states of the cluster through a Schrieffer–Wolff transformation<sup>52</sup> to get

$$J = 2t^2 \sum_{\nu\sigma} \frac{\langle \uparrow | c_{\Delta\sigma}^\dagger | \nu \rangle \langle \nu | c_{\Delta\sigma} | \downarrow \rangle + \langle \uparrow | c_{\Delta\sigma} | \nu \rangle \langle \nu | c_{\Delta\sigma}^\dagger | \downarrow \rangle}{E_\nu - E_\uparrow} \quad (11)$$

where  $|\sigma\rangle$  is the degenerate ground state of the cluster with energy  $E_\uparrow = E_\downarrow$ , and the  $|\nu\rangle$  are excited states. Note that in the absence of electron-hole symmetry in the cluster there will also be a local potential scattering for the conduction electrons due to the cluster.

Figure 9(a) shows the  $J$ -coupling in the  $[\varepsilon_H, V]$  plane while Fig. 9(b) shows its dependence on  $V$  for different values of  $\varepsilon_H$ . For small  $V \ll t$ , the magnetic moment, which is mainly localized on the H atom, is weakly coupled to the graphene sheet and the Kondo coupling is small. For a fixed  $V$ , the Kondo coupling increases as  $\varepsilon_H$  approaches the charge degeneracy lines where perturbation theory fails and so  $J$  diverges due to vanishing denominators in Eq. (11). For large  $V > 2t$  the bond between the H atom and the C<sub>0</sub> atom is strong enough to effectively decouple both atoms from the rest of the system. The magnetic moment is transferred to the  $|\Delta\rangle$  state and the Kondo coupling becomes  $V$  independent. In the large  $V$  limit it is simply given by  $J(V \rightarrow \infty) = 8t^2/U_\Delta = 24t$ .

We complete the analysis by coupling the cluster to the rest of the graphene layer which provides an hybridization  $\Gamma_\Delta \sim \sqrt{3}|\omega|$  at low energies. In the parameter region where the cluster is magnetic, we end-up with a pseudo-gap Kondo problem.<sup>19,53–62</sup> In this model, for an electron-hole symmetric impurity, the magnetic moment of the impurity (the cluster in the present case) remains unscreened even at zero temperature. For the electron-hole asymmetric situation the magnetic moment can be screened only if the Kondo coupling is larger than a critical coupling  $J_c$  of the order of the bandwidth.<sup>53,54</sup> We calculated the stability of the magnetic moment in the cluster when it is coupled to the rest of the system. We used the NRG<sup>63,64</sup> with a pseudo-gapped density of states and a Fermi velocity chosen to reproduce the effect of  $\Sigma_\Delta(\omega)$ .

The solid line in Fig. 9(a) shows the NRG results for the stability region of the total magnetic moment on the cluster at zero temperature. We observe that the coupling to the rest of the system reduces the parameter area where the magnetic moment is stable at zero temperature (a similar effect is observed in the Hartree-Fock solution). For  $V \lesssim 2t$  the magnetic moment is mainly localized on the H atom and it is screened when the Kondo coupling reaches a critical value of  $\sim 10t$  (this unconventional screening is associated to a change of the cluster's charge<sup>61</sup>). For larger values of  $V$  the magnetic moment is localized on the  $|\Delta\rangle$  state. At finite but large ( $> 2t$ ) values of  $V$  the critical coupling increases with increasing  $V$ . This is due to the fact that, in the present model, if  $V \rightarrow \infty$  the

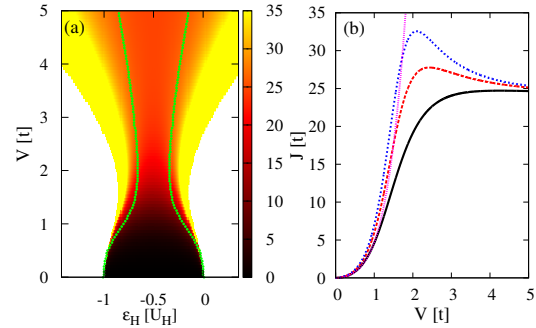


FIG. 9. (Color online) Kondo coupling constant  $J$  estimated from the exact diagonalization of the MAHM cluster. (a) as a function of  $\varepsilon_H$  and  $V$  and for the same parameters as in Fig. 8. (b)  $J$  as a function of  $V$  for three different values of  $\varepsilon_H$ :  $-U_H/2$  (solid line),  $-0.8t$  (dashed line) and  $-0.7t$  (short-dashed line). The case  $U_C = 0$  (dotted line) is included for comparison.

magnetic impurity becomes electron-hole symmetric for any value of  $\varepsilon_H$  and the magnetic moment remains unscreened for any value of  $J$ .

It is worth mentioning that in the doped case the magnetization maps of Fig. 8 are modified.<sup>14</sup> For  $V \gtrsim 2t$ , the magnetic moment stability region narrows and shifts, being centered around a line given by  $V^2 \sim a\varepsilon_H + b$ . This shows that the impurity states is much more sensitive to doping in the vacancy-like regime than in the low  $V$  regime where the magnetic moment is localized at the H atom. Therefore, a realistic H induced defect on graphene would be more sensitive to doping than what one would expect from the usual Anderson-like model for an impurity on pristine graphene. A detailed study of this effect will be presented elsewhere.

## V. SUMMARY AND CONCLUSIONS

We have combined a DFT description of diluted H impurities on graphene with tight-binding and effective models to describe the magnetic structure of a H induced defect. The DFT approach provides a realistic picture of the structural distortions around the adsorbed H atom and predicts a magnetic moment localized in the neighborhood of the adatom. Additionally, it allows us to estimate parameters that are used to build an effective Anderson-Hubbard type model Hamiltonian. The model is solved at the mean-field level and the results are compared with the full DFT band structure to test the quality of the mapping. The model Hamiltonian is then used to study a *single* H impurity adsorbed on graphene, a situation that can not be tackled with the current DFT based methods and that allows us to identify in detail the structure of the induced defect as well as its magnetic properties without the complications generated by the interactions between impurities.

Within the single impurity Anderson-Hubbard Hamilto-

nian, the mean field approximation gives a magnetic solution for undoped graphene and a strong dependence of the impurity magnetic moment with doping—an effect with interesting implications for spintronics and for applications in magneto-transport devices.

In order to treat the delicate balance between kinetic energy and correlations at the defect including quantum fluctuations, we devised a minimal Anderson-Hubbard model that takes into account explicitly the electronic correlations at the impurity orbital as well as on the surrounding carbon atoms and replace the rest of the system by an effective medium.

An analysis of the isolated cluster illustrates the structure of the magnetic moment. For  $-U_H < \varepsilon_H < 0$  and small hybridization  $V$  the spin is localized at the H orbital while for large  $V$  the spin is transferred to the carbon atoms forming a vacancy-like state. For intermediate values of the hybridization, that correspond to a realistic description of H, the stability region shows a neck and the magnetic moment is in a linear combination of the impurity and C orbitals. The effect of the rest of the host graphene is treated as an effective medium with a pseudo-gap using the NRG. We consider the case of undoped graphene where the Fermi energy lies at the Dirac point. As shown in Fig. 9 the region of stability of the magnetic moment is narrowed as the cluster is coupled to the rest of the system. This behavior can be understood in terms of the known results for the Anderson impurity model in a system with a graphene-like pseudo-gap: in the case of electron-hole symmetry the spin is never screened,<sup>54</sup> while away from the electron-hole symmetry the spin can be screened at low temperatures if the Kondo coupling is larger than a critical value of the order of the bandwidth. Interestingly, within our model, in the large  $V$  regime (vacancy-like state), the electron-hole symmetry is recovered and the magnetic moment remains unscreened.

While breaking the electron-hole symmetry will modify some of these results (a detailed study will be presented elsewhere), the main results of the present work are robust against it: (i) the spin is transferred to the carbon atoms as the hybridization increases, (ii) the Kondo coupling can reach quite large values, and (iii) for realistic values of the parameters (obtained from our DFT calculations) the H induced defect is half-way between the one corresponding to an adatom weakly coupled to pristine graphene and a carbon vacancy.

## ACKNOWLEDGMENTS

We thank M. Vojta and T. Wehling for useful conversations. JOS and AS acknowledge support from the Donors of the American Chemical Society Petroleum Research Fund and use of facilities at the Penn State Materials Simulation Center. GU, PSC, ADH, and CAB acknowledge financial support from PICTs 06-483 and 2008-2236 from ANPCyT and PIP 11220080101821 from CONICET, Argentina.

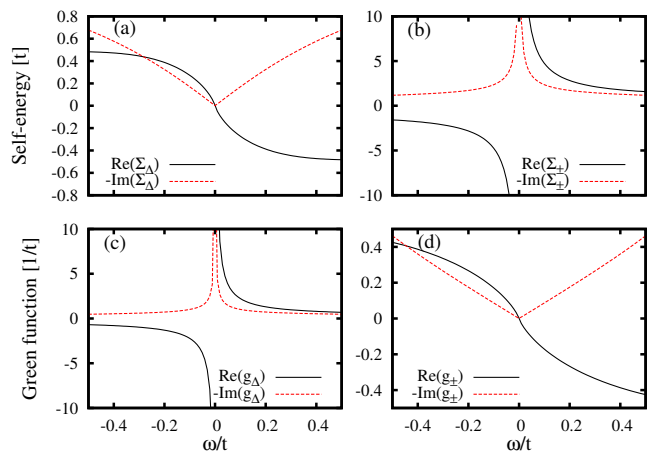


FIG. 10. Self-energy and unperturbed green functions of the  $C_n$  atoms. (a) and (c) correspond to the state  $|\Delta\rangle$  while (b) and (d) correspond to the  $|\pm\rangle$  states. Note that  $\Sigma_\Delta(\omega)$  presents a pseudo-gap close to the Dirac Point, and then  $g_\Delta(\omega)$  shows a resonant-like behavior (vacancy state). The opposite behavior is observed for  $\Sigma_\pm(\omega)$  and  $g_\pm(\omega)$ .

## Appendix A: Non-interacting self-energy

In Section III we solved the adatom problem using a simplified model where Coulomb interaction was assumed to be relevant only on the  $C_0$  and  $C_n$  carbon atoms. In that case, and if we are only interested on the properties of the reduced system formed by the adatom and the above mentioned  $C$  atoms, the presence of the rest of the graphene sheet can be taken into account through a self-energy contribution. In the following, we calculate this self-energy using the Dyson equation and taking advantage of the following: (i) the structure of the honeycomb lattice around a given atom has the same structure of a Bethe lattice (up to the second nearest-neighbors) which allows a simple disentanglement of the lattice Green function; (ii) the exact lattice Green function of a given site,  $\mathcal{G}_i$  of the honeycomb lattice has an analytic closed form.<sup>65</sup>

Let us denote by  $c_\Delta^\dagger = \sum_i c_i^\dagger / \sqrt{3}$  the fermionic operator that creates an electron in a state that is a symmetric linear combination of the  $p_z$  orbitals of the three nearest-neighbors atoms of  $C_0$ . The quantity of interest is the non-interacting self-energy of that state  $\Sigma_\Delta(\omega)$  due to the rest of the graphene (without  $C_0$ ). That is, if  $g_\Delta(\omega) = \langle\langle c_\Delta, c_\Delta^\dagger \rangle\rangle$  denotes the retarded Green function *in the absence* of the coupling with  $C_0$ , then  $\Sigma_\Delta(\omega) = \omega - g_\Delta^{-1}(\omega)$ . The Dyson equation,  $\mathcal{G} = g + g \mathbf{V} \mathcal{G}$ , relates the unperturbed Green function  $g$  with the Green function  $\mathcal{G}$  in the presence of the perturbation  $\mathbf{V}$ . Taking the hopping between the site “0” and its three nearest-neighbors as the perturbation, we can immediately obtain the following expression for the Green function of the site “0” (corresponding to the  $p_z$ -orbital of  $C_0$ ),

$$\mathcal{G}_0 = g_0 + g_0 3t^2 \mathcal{G}_0 g_\Delta \quad (\text{A1})$$

where  $g_0(\omega) = (\omega + i0^+)^{-1}$  and<sup>66</sup>

$$\mathcal{G}_0(\omega) = \frac{\omega}{2\pi t^2} \mathcal{S}\left(\frac{\omega^2 - 3t}{2t}\right) \mathcal{Q}\left(\frac{\omega^2 - 3t}{2t}\right) \quad (\text{A2})$$

with

$$\mathcal{S}(x) = 8(\sqrt{2x+3} - 1)^{-\frac{3}{2}}(\sqrt{2x+3} + 3)^{-\frac{1}{2}}. \quad (\text{A3})$$

and

$$\mathcal{Q}(x) = \begin{cases} K(k(x)^2) & \text{if } \text{Im}(x) \text{Im}(k) < 0 \\ K(k(x)^2) + 2i p(x) K(1 - k(x)^2) & \text{otherwise} \end{cases} \quad (\text{A4})$$

with  $K(k)$  the complete elliptic integral of the first kind,  $p(x) = \text{sign}(\text{Im}(x))$  and  $k(x) = (2x+3)^{1/4} \mathcal{S}(x)/2$ . After some straightforward algebra we finally get

$$\Sigma_{\Delta}(\omega) = \omega - \frac{3t^2}{\Sigma_0(\omega)} \quad (\text{A5})$$

where  $\Sigma_0(\omega) = \omega - \mathcal{G}_0^{-1}(\omega)$ . We notice that, in the low energy limit ( $|\omega| \rightarrow 0$ ),

$$-\text{Im}(\Sigma_{\Delta}(\omega)) \simeq -3t^2 \text{Im}(\mathcal{G}_0(\omega)) = \sqrt{3} |\omega|. \quad (\text{A6})$$

This shows that the effective density of states of the part of the graphene sheet that couples to the symmetric state defined above also presents a pseudo-gap and goes linearly to zero [see Fig. 10(a)].

A similar analysis can be done for the green function and the self-energy corresponding to the  $|\pm\rangle$  states,  $g_{\pm}(\omega)$  and  $\Sigma_{\pm}(\omega)$ , respectively. We then obtain

$$g_{\pm}(\omega) = \frac{3}{2} \mathcal{G}_0(\omega) - \frac{1}{2} \mathcal{G}_{\Delta}(\omega) \quad (\text{A7})$$

and

$$\Sigma_{\pm}(\omega) = \omega - g_{\pm}^{-1}(\omega) \quad (\text{A8})$$

with  $\mathcal{G}_{\Delta}(\omega) = [\omega - \Sigma_{\Delta}(\omega) - 3t^2 g_0(\omega)]^{-1}$ . This functions are plotted in Figs. 10(b) and 10(d).

From these results, it is clear that, at low energies, the  $|\Delta\rangle$  state is only weakly coupled to the rest of the graphene sheet (excluding  $C_0$ ) while the opposite is true for the other two orthogonal states  $|\pm\rangle$ . This justifies our simplified model described in Section III.

- 
- <sup>1</sup> K. S. Novoselov, A. K. Geim, S. V. Morozov, D. Jiang, M. I. Katsnelson, I. V. Grigorieva, S. V. Dubonos, and A. A. Firsov, *Nature* **438**, 197 (2005).
- <sup>2</sup> M. I. Katsnelson, K. S. Novoselov, and A. K. Geim, *Nat. Phys.* **2**, 620 (2006).
- <sup>3</sup> K. S. Novoselov, Z. Jiang, Y. Zhang, S. V. Morozov, H. L. Stormer, U. Zeitler, J. C. Maan, G. S. Boebinger, P. Kim, and A. K. Geim, *Science* **315**, 1379 (2007).
- <sup>4</sup> A. K. Geim and K. S. Novoselov, *Nat. Mat.* **6**, 183 (2007).
- <sup>5</sup> A. H. Castro Neto, F. Guinea, N. M. R. Peres, K. S. Novoselov, and A. K. Geim, *Rev. Mod. Phys.* **81**, 109 (2009), and refs. therein.
- <sup>6</sup> S. Das Sarma, S. Adam, E. H. Hwang, and E. Rossi, *Rev. Mod. Phys.* **83**, 407 (2011).
- <sup>7</sup> K. S. Novoselov, A. K. Geim, S. V. Morozov, D. Jiang, Y. Zhang, S. V. Dubonos, I. V. Grigorieva, and A. A. Firsov, *Science* **306**, 666 (2004).
- <sup>8</sup> Y. Zhang, Y.-W. Tan, H. L. Stormer, and P. Kim, *Nature* **438**, 201 (2005).
- <sup>9</sup> P. R. Wallace, *Phys. Rev.* **71**, 622 (1947).
- <sup>10</sup> P. O. Lehtinen, A. S. Foster, A. Ayuela, A. Krasheninnikov, K. Nordlund, and R. M. Nieminen, *Phys. Rev. Lett.* **91**, 017202 (2003).
- <sup>11</sup> E. J. Duplock, M. Scheffler, and P. J. D. Lindan, *Phys. Rev. Lett.* **92**, 225502 (2004).
- <sup>12</sup> J. C. Meyer, C. O. Girit, M. F. Crommie, and A. Zettl, *Nature* **454**, 319 (2008).
- <sup>13</sup> K. T. Chan, J. B. Neaton, and M. L. Cohen, *Phys. Rev. B* **77**, 235430 (2008).
- <sup>14</sup> B. Uchoa, V. N. Kotov, N. M. R. Peres, and A. H. Castro Neto, *Phys. Rev. Lett.* **101**, 026805 (2008).
- <sup>15</sup> A. H. Castro Neto and F. Guinea, *Phys. Rev. Lett.* **103**, 026804 (2009).
- <sup>16</sup> D. W. Boukhvalov, M. I. Katsnelson, and A. I. Lichtenstein, *Phys. Rev. B* **77**, 035427 (2008).
- <sup>17</sup> D. W. Boukhvalov and M. I. Katsnelson, *Journal of Physics: Condensed Matter* **21**, 344205 (2009).
- <sup>18</sup> A. Castro Neto, V. Kotov, J. Nilsson, V. Pereira, N. Peres, and B. Uchoa, *Solid State Comm.* **149**, 1094 (2009).
- <sup>19</sup> P. S. Cornaglia, G. Usaj, and C. A. Balseiro, *Phys. Rev. Lett.* **102**, 046801 (2009).
- <sup>20</sup> T. O. Wehling, M. I. Katsnelson, and A. I. Lichtenstein, *Phys. Rev. B* **80**, 085428 (2009).
- <sup>21</sup> T. O. Wehling, A. V. Balatsky, M. I. Katsnelson, A. I. Lichtenstein, and A. Rosch, *Phys. Rev. B* **81**, 115427 (2010).
- <sup>22</sup> T. O. Wehling, H. P. Dahal, A. I. Lichtenstein, M. I. Katsnelson, H. C. Manoharan, and A. V. Balatsky, *Phys. Rev. B* **81**, 085413 (2010).
- <sup>23</sup> Z. M. Ao and F. M. Peeters, *Appl. Phys. Lett.* **96**, 253106 (2010).
- <sup>24</sup> A. D. Hernández-Nieves, B. Partoens, and F. M. Peeters, *Phys. Rev. B* **82**, 165412 (2010).
- <sup>25</sup> K. T. Chan, H. Lee, and M. L. Cohen, *Phys. Rev. B* **84**, 165419 (2011).
- <sup>26</sup> N. Tombros, C. Jozsa, M. Popinciuc, H. T. Jonkman, and B. J. van Wees, *Nature* **448**, 571 (2007).
- <sup>27</sup> O. V. Yazyev and M. I. Katsnelson, *Phys. Rev. Lett.* **100**, 047209 (2008).
- <sup>28</sup> M. Wimmer, İnanç Adagideli, S. Berber, D. Tománek, and K. Richter, *Phys. Rev. Lett.* **100**, 177207 (2008).
- <sup>29</sup> G. Usaj, *Phys. Rev. B* **80**, 081414(R) (2009).
- <sup>30</sup> D. Soriano, F. Muñoz-Rojas, J. Fernández-Rossier, and J. J. Palacios, *Phys. Rev. B* **81**, 165409 (2010).
- <sup>31</sup> C. Józsa, M. Popinciuc, N. Tombros, H. T. Jonkman, and B. J. van Wees, *Phys. Rev. B* **79**, 081402 (2009).
- <sup>32</sup> W. Han, K. Pi, K. M. McCreary, Y. Li, J. J. I. Wong, A. G. Swartz, and R. K. Kawakami, *Phys. Rev. Lett.* **105**, 167202 (2010).

- <sup>33</sup> O. V. Yazyev and L. Helm, Phys. Rev. B **75**, 125408 (2007).
- <sup>34</sup> J. J. Palacios, J. Fernández-Rossier, and L. Brey, Phys. Rev. B **77**, 195428 (2008).
- <sup>35</sup> O. V. Yazyev, Phys. Rev. Lett. **101**, 037203 (2008).
- <sup>36</sup> R. Balog, B. Jørgensen, J. Wells, E. Lægsgaard, P. Hofmann, F. Besenbacher, and L. Hornekær, J. Am. Chem. Soc. **131**, 8744 (2009).
- <sup>37</sup> O. V. Yazyev, Rep. Prog. Phys. **73**, 056501 (2010).
- <sup>38</sup> P. Haase, S. Fuchs, T. Pruschke, H. Ochoa, and F. Guinea, Physical Review B **83**, 241408 (2011).
- <sup>39</sup> S. Casolo, O. M. Lovvik, R. Martinazzo, and G. F. Tantardini, J. Chem. Phys. **130**, 054704 (2009).
- <sup>40</sup> D. C. Elias, R. R. Nair, T. M. G. Mohiuddin, S. V. Morozov, P. Blake, M. P. Halsall, A. C. Ferrari, D. W. Boukhvalov, M. I. Katsnelson, A. K. Geim, and K. S. Novoselov, Science **323**, 610 (2009).
- <sup>41</sup> V. M. Pereira, F. Guinea, J. M. B. L. dos Santos, N. M. R. Peres, and A. H. C. Neto, Phys. Rev. Lett. **96**, 036801 (2006).
- <sup>42</sup> J.-H. Chen, L. Li, W. G. Cullen, E. D. Williams, and M. S. Fuhrer, Nature Physics **7**, 535 (2011).
- <sup>43</sup> There is, however, some controversy in the literature regarding whether the value of  $U_C$  is closer to the critical value that would generate a magnetic instability in pure graphene.<sup>67</sup> Within the context of DFT, we used the *Quantum Espresso* package<sup>68</sup> to obtain  $U_C \sim 3.2 - 3.5\text{eV}$ .
- <sup>44</sup> G. Kresse and J. Furthmüller, Computational Materials Science **6**, 15 (1996); G. Kresse and J. Furthmüller, Phys. Rev. B **54**, 11169 (1996).
- <sup>45</sup> P. E. Blöchl, Phys. Rev. B **50**, 17953 (1994).
- <sup>46</sup> G. Kresse and D. Joubert, Phys. Rev. B **59**, 1758 (1999).
- <sup>47</sup> J. P. Perdew, K. Burke, and M. Ernzerhof, Phys. Rev. Lett. **77**, 3865 (1996).
- <sup>48</sup> J. P. Perdew, K. Burke, and M. Ernzerhof, Phys. Rev. Lett. **78**, 1396 (1997).
- <sup>49</sup> J. Neugebauer and M. Scheffler, Phys. Rev. B **46**, 16067 (1992); G. Makov and M. C. Payne, Phys. Rev. B **51**, 4014 (1995).
- <sup>50</sup> J. O. Sofo, A. M. Suarez, G. Usaj, P. S. Cornaglia, A. D. Hernández-Nieves, and C. A. Balseiro, Phys. Rev. B **83**, 081411 (2011).
- <sup>51</sup> N. M. R. Peres, F. Guinea, and A. H. Castro Neto, Phys. Rev. B **73**, 125411 (2006).
- <sup>52</sup> J. Schrieffer and P. Wolff, Phys. Rev. **149**, 491 (1966).
- <sup>53</sup> D. Withoff and E. Fradkin, Phys. Rev. Lett. **64**, 1835 (1990).
- <sup>54</sup> L. Fritz and M. Vojta, Phys. Rev. B **70**, 214427 (2004).
- <sup>55</sup> D. Jacob and G. Kotliar, Phys. Rev. B **82**, 085423 (2010).
- <sup>56</sup> K. Ingersent, Phys. Rev. B **54**, 11936 (1996).
- <sup>57</sup> M. Vojta, L. Fritz, and R. Bulla, Europhys. Lett. **90**, 27006 (2010).
- <sup>58</sup> R. Bulla, T. Pruschke, and A. C. Hewson, Journal of Physics: Condensed Matter **9**, 10463 (1999).
- <sup>59</sup> K. Chen and C. Jayaprakash, Journal of Physics: Condensed Matter **7**, L491 (1999).
- <sup>60</sup> L. Fritz, S. Florens, and M. Vojta, Phys. Rev. B **74**, 144410 (2006).
- <sup>61</sup> M. Vojta and L. Fritz, Phys. Rev. B **70**, 094502 (2004).
- <sup>62</sup> B. Uchoa, T. G. Rappoport, and A. H. Castro Neto, Phys. Rev. Lett. **106**, 016801 (2011).
- <sup>63</sup> K. Wilson, Rev. Mod. Phys. **47**, 773 (1975).
- <sup>64</sup> R. Bulla, T. A. Costi, and T. Pruschke, Rev. Mod. Phys. **80**, 395 (2008).
- <sup>65</sup> T. Horiguchi, J. Math. Phys. **13**, 1411 (1972).
- <sup>66</sup> Here, it is understood that  $\mathcal{G}_0$  is evaluated with an infinitesimal imaginary part,  $\mathcal{G}_0(\omega + i0^+)$ .
- <sup>67</sup> T. O. Wehling, E. Şaşıoğlu, C. Friedrich, A. I. Lichtenstein, M. I. Katsnelson, and S. Blügel, Phys. Rev. Lett. **106**, 236805 (2011).
- <sup>68</sup> M. Cococcioni and S. de Gironcoli, Phys. Rev. B **71**, 035105 (2005).